SLM 2D Model

M.J. ARENAS[1] D. HÖMBERG[1] M. ROSIÈRE[1]

[1] Technische Universität Berlin
Institut für Mathematik
arenas@math.tu-berlin.de

hoemberg@wias-berlin.de

rosiere@math.tu-berlin.de

May 20, 2022

Abstract

Simplified model for 3D printing with Selective Laser Melting (SLM). It consists on a 2D model. SLM is also known as Laser Powder Bed Fusion (L-PBF) = Direct Metal Laser Melting (DMLM). The domain is a cross-section of the structure being built. Each new layer consist of metallic powder material. The laser is moving and heating a specific are which melts and solidifies. This later effect is considered with a phase evolutionary equation. Some important features are: heat equation, phase equation (powder/solid state), laser movement.

I. DOMAIN DESCRIPTION

The computational domain Ω consists of a platform Ω_0, also known as substrate, and the layers of powder material Ω_i for $i = 1,\dots,n$ located on top of it. The powder layers are deposited one by one, that is, one per cycle. A cycle consists of the deposition of a whole layer of powder and laser pass. In this report, the model will be 2D. It can be understood as a cross-section of a 3D domain comprising the substrate and powder layers.

The height of the platform Ω_0 is h_0 while the length is l. As the main interest in the process is on the powder layers, the platform is below the origin of coordinates, from $-h_0$ to 0, while the powder layers are above it. To keep the symmetry in width, the platform is located from $-l/2$ until $l/2$. This way,

$$\Omega_0 = [-h_0, 0] \times [-l/2, l/2]. \tag{1}$$

Each powder layer Ω_i instead will have a height h which is way smaller than h_0. The width of the layer can be considered to be equal or smaller than the width of the platform. This way, each Ω_i can be defined as

$$\Omega_i = [(i-1)h, ih] \times [-l/2, l/2] \quad i = 1,\dots,n. \tag{2}$$

The index i represents the number of the layer which at the same time corresponds with the laser cycle. Therefor, the whole domain Ω changes with time. The domain Ω at the level k is defined as Ω^k as follows:

$$\Omega = \Omega^k = \bigcup_{i=0}^{k} \Omega_i. \tag{3}$$

Specifically,

$$\Omega^k = [-h_0, 0[\cup [0, kh] \times [-l/2, l/2] \quad k = 0,\dots,n. \tag{4}$$

A graphical representation of the domain Ω and subdomains Ω_i can be seen in Figure 1.

As the domain Ω changes with time, the boundaries also do. The boundaries will be divided into vertical (left/right) and horizontal (top/bottom) and will be denoted as Σ and Γ respectively.

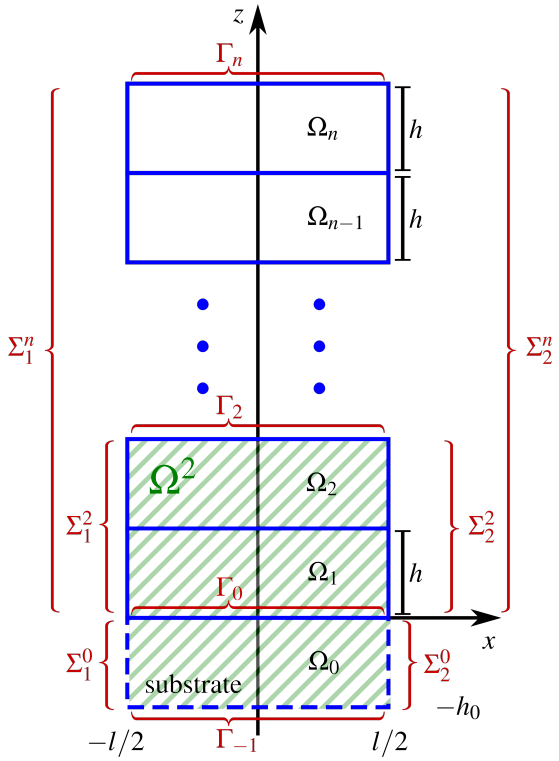

Figure 1: *Domain.*

- Horizontal (Top and bottom):

$$\Gamma_i = \left\{(x,z) \in \Omega^i : z = ih\right\} \tag{5}$$
$$\Gamma_0 = \{(x,z) \in \Omega : z = 0\} \tag{6}$$
$$\Gamma_{-1} = \{(x,z) \in \Omega : z = -h_0\} \tag{7}$$

Boundary conditions:

$$-\kappa\frac{\partial\theta}{\partial n} = \alpha_1(\theta - \theta_a) \qquad \text{at } \Gamma_i \tag{8}$$
$$-\kappa\frac{\partial\theta}{\partial n} = 0 \qquad \text{at } \Gamma_{-1} \tag{9}$$
$$\text{or}$$
$$\theta = \theta_a \qquad \text{at } \Gamma_{-1} \tag{10}$$

- Vertical (Sides):

$$\Sigma_1^0 = \{(x,z) \in \Omega : x = -l/2, z \in \Omega_0\} \tag{11}$$
$$\Sigma_2^0 = \{(x,z) \in \Omega : x = l/2, z \in \Omega_0\} \tag{12}$$
$$\Sigma_i^0 = \left\{(x,z) \in \Omega : x = (-1)^i l/2, z \in \Omega_0\right\} \text{ for } i = 1,2. \tag{13}$$

$$\Sigma_1^n = \{(x,z) \in \Omega : x = -l/2, z \in \Omega_n \setminus \Omega_0\} \tag{14}$$
$$\Sigma_2^n = \{(x,z) \in \Omega : x = l/2, z \in \Omega_n \setminus \Omega_0\} \tag{15}$$
$$\Sigma_i^n = \left\{(x,z) \in \Omega : x = (-1)^i l/2, z \in \Omega_n \setminus \Omega_0\right\} \text{ for } i = 1,2. \tag{16}$$

Boundary conditions:

$$-\kappa\frac{\partial\theta}{\partial n} = \alpha_2(\theta - \theta_a) \qquad \text{for } x \in \Sigma_i^n \text{ for } i = 1,2. \tag{17}$$
$$-\kappa\frac{\partial\theta}{\partial n} = \alpha_3(\theta - \theta_a) \qquad \text{for } x \in \Sigma_i^0 \text{ for } i = 1,2. \tag{18}$$
$$\tag{19}$$

IS THIS NECESSARY?
Interface condition between substrate and layers (at Γ_0):

$$\text{at } \Gamma_0(z=0) : \begin{cases} [\theta] &= \sigma \\ [-\kappa\dfrac{\partial\theta}{\partial z}] &= \sigma \end{cases} \tag{20}$$

More information on boundary conditions for a SLM Model can be found in [1].

II. TIME DISCRETIZATION

The entire printing process requires a time period of T seconds. This time period is be subdivided into cycles. A cycle consist on the immediate deposition of a new powder layer on top of the previous layer and the time

it is affected by the laser. For now, let us consider that each cycle lasts the same time τ seconds. This way, the discretization on time to build a structure Ω^n with n layers is the following:

$$[0,T] = \bigcup_{i=1}^{n} [(i-1)\tau, i\tau]. \tag{21}$$

III. Governing equations

The main purpose of the model is to track the temperature distribution during the printing process. Thus, the evolutionary heat equation will play a main role. For this, it is necessary to take into account the material properties of the domain changing with the materials. That is mainly, the platform, the metallic powder and the solidified structure. To consider the change from powder to solidified material, we will take the approach of a phase change. A system of ordinary differential equations are usually employed to consider the changes in the concentration of the solid phases of steel. [2, 3, 4, 5, 6, 7, 8]

Similarly we want to develop a system to consider the transition from metallic powder to solidified material passing through melting/liquefaction. Furthermore it is interesting in the case of steel powder to consider the solid-solid phase changes from steel solidified material into austenite, bainite, martensite,... See Figure 2.

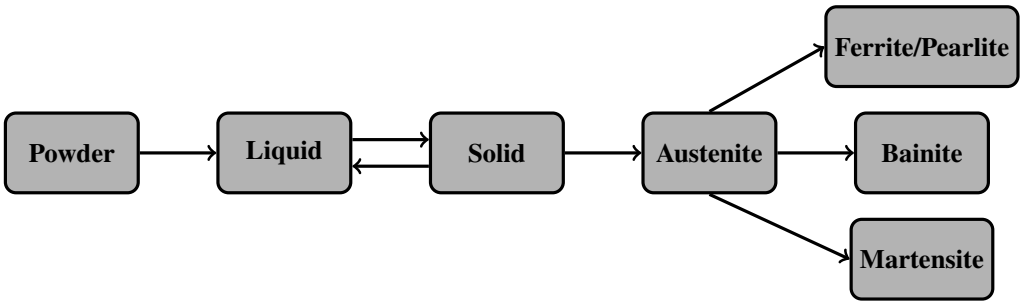

Figure 2: *Diagram with phases changes during SLM of steel powder.*

i. Heat equation

We can know the heat distribution during the SLM by solving the following heat equation:

$$\rho C_p \theta_t - \nabla \cdot (\kappa \nabla \theta) = \phi(t) \quad \text{on } \Omega \times [0,T]. \tag{22}$$

This problem can be subdivided using the cycles. For $i = 1$ to n, solve

$$\rho C_p \theta_t - \nabla \cdot (\kappa \nabla \theta) = \phi(t) \quad \text{on } \Omega^i \times [(i-1)\tau, i\tau]. \tag{23}$$

In both cases subject to boundary conditions (8)-(9) and (17)-(18), (??? interface condition to substrate (20)???) and initial conditions:

$$\theta = \theta_a \qquad \text{at } t = 0 \tag{24}$$

and

$$\theta = \theta_a \qquad \text{at } t = (i-1)\tau \text{ on } \Omega_i \text{ for } i = 1, ..., n \tag{25}$$

It has to be noticed that to make the model with the initial conditions for each cycle consistent when using (23) the following must be fulfilled: if we notate the final temperature field of the cycle i in Ω^i as $\theta(t = i\tau)$, then the initial conditions for the cycle $i+1$ are

$$\theta = \theta(t = i\tau) \qquad \text{at } t = i\tau \text{ on } \Omega^{i+1} \setminus \Omega_{i+1} \tag{26}$$

and

$$\theta = \theta_a \qquad \text{at } t = i\tau \text{ on } \Omega_{i+1}. \tag{27}$$

ii.Phase equations

Main references [7, 8].

ii.1 Powder into Liquid/Solid

First, let us consider the study of one single phase transition. From metallic powder into solid. We neglect any transition time from melting to cooling. Under this assumption, the liquid/melting phase is calculated and is turned into solid immediately. Essentially, for notation purposes the liquid phase and solid phase are equivalent.

As we are studying the growth of solid phase, and no solid can turn into powder, under the previous assumption it is reasonable to consider one single phase equation. The variable z will be used to describe the fraction/concentration of solid phase material with values from 0 to 1. Meaning that powder is equivalent to $z = 0$ and solid to $z = 1$.

The ordinary differential equation describing the growth of solid phase can defined as

$$\dot{z} = f_z(\theta, z) \tag{28}$$

The function f_z requires a proper definition such that the growth happens quickly, the solid phase fraction z is between 0 and 1 and the growth of the solid phase fraction can only happen from metallic powder (so no platform material can turn into solid phase, or solid phase into solid phase). A summary of this model is represented in Figure 3.

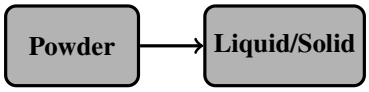

Figure 3: *Diagram for a single phase transition.*

TEST1:

$$f_z(\theta, z) = \frac{1}{\tau_z}\mathscr{H}(\theta - \theta_m) \tag{29}$$

- τ_z: transformation velocity
- $\mathscr{H}$: Heaviside function
- θ_m: melting temperature

Although this function is useful to see where the solid phase growths, the values of z go outside of the desired range $[0,1]$. For example, the solid phase keeps growing in a region where there is already a concentration of solid phase of 1. See Figure 4.

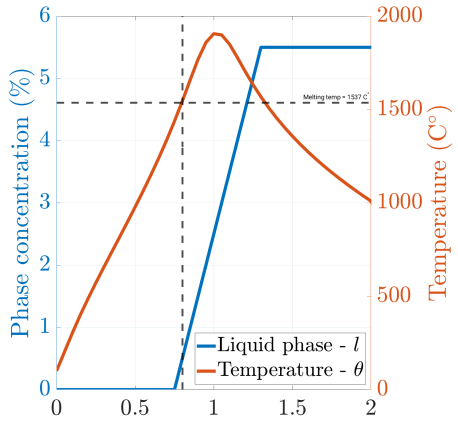

Figure 4: *Test 1: Phase evolution vs temperature during printing process.*

TEST2:

$$f_z(\theta, z) = \frac{1}{\tau_z}[\mathscr{H}(\theta - \theta_m) - z]_+ \tag{30}$$

- τ_z: transformation velocity
- $\mathscr{H}$: Heaviside function
- θ_m: melting temperature
- $[.]_+$: positive part function

Equation 30 is a modification of equation (29). The $-z$ term stops the growth of the phase if the phase has achieved a concentration of 1. That is, cancelling the Heaviside term. With the positive part function we do not allow the phase to decrease. See Figure 5 for different values of τ_z. Notice that for computational purposes, the value of τ_z should not exceed the value of Δt.

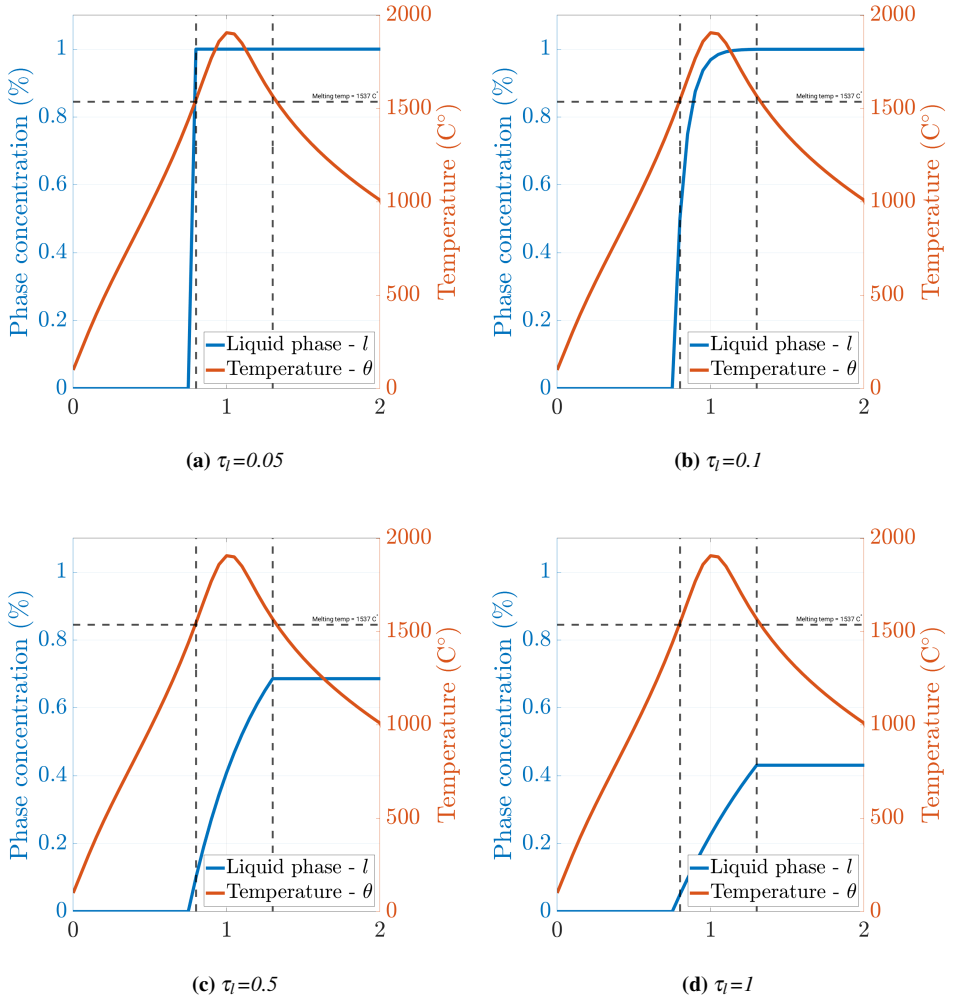

(a) τ_l=0.05 **(b)** τ_l=0.1

(c) τ_l=0.5 **(d)** τ_l=1

Figure 5: *Test 2: Phase evolution vs temperature during printing process. Different values of* τ_l.

ii.2 Powder into Liquid into Solid

As the second step, let us consider two phases: liquid/molten phase and solid phase. We keep the transition from powder to melting phase which occurs when the powder is over the melting temperature and we add the solidification of the melting phase.

Thus, the deposited powder layer is affected by the laser scan. The areas where melting temperature is achieved will have liquid phase growth. After the pass of the laser, cooling happens. When the liquid phase is below the solidification temperature, it will turn into the solid phase.

When a new powder layer is deposited on top of a previous layer, the heat of the laser may reach the previous layer, which already has solid phase. This solid phase is remelted and consequently turns into liquid. This way, the model must be valid for more than one heating and cooling cycle.

A summary of this model is represented in Figure 6.

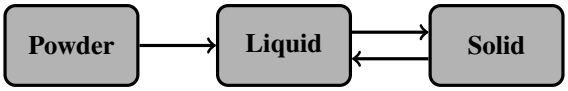

Figure 6: *Diagram for heating and cooling transitions.*

System of equations:

We consider the liquid phase l and the solid phase s in the model. The model is based on [7] where the liquid phase and the solid phase take the roles of austenite (heating) and martensite (cooling) respectively. This way the system of equations is the following:

$$\dot{l} = \frac{1}{\tau_l}[l_{eq}(\theta) - l]_+ - \dot{s} \tag{31}$$

$$\dot{s} = \frac{1}{\tau_s}[s_{eq}(\theta) - s]_+ - \dot{l}. \tag{32}$$

The equilibrium fractions of liquid and solid phase are defined as follows:

$$l_{eq}(\theta) = \mathscr{H}(\theta - \theta_m) \tag{33}$$

$$s_{eq}(\theta) = \min\{s_{MK}(\theta), s + l\} \tag{34}$$

$$s_{MK}(\theta) = 1 - e^{-c_{km}(\theta_s - \theta)} \tag{35}$$

The liquid equilibrium fraction l_{eq} is the function used in the previous section. This function could be further regularized/smoothed by using a regularized version of the Heaviside function. This is more appropriate if we consider that the melting transformation is not full once the θ_m value is reached. Instead, there is a initiation melting temperature where a mushy zone is generated.

The solid equilibrium function s_{eq} is defined using the Koistinen and Marburger formula [7, 9]. Upon cooling, owing to the positive part function , the first term on the right hand side of (31) becomes zero and the volume fraction is decreased due to the growth of the solid phase expressed in (32).

At any time the maximal volume fraction of solid that can be produced is given by the sum $s + l$, i.e., the amount which has been produced so far and the remaining fraction of liquid phase.

- τ_z: transformation velocity
- $\mathscr{H}$: Heaviside function
- θ_m: melting temperature
- θ_s: solidification temperature
- $[.]_+$: positive part function

Matlab results:

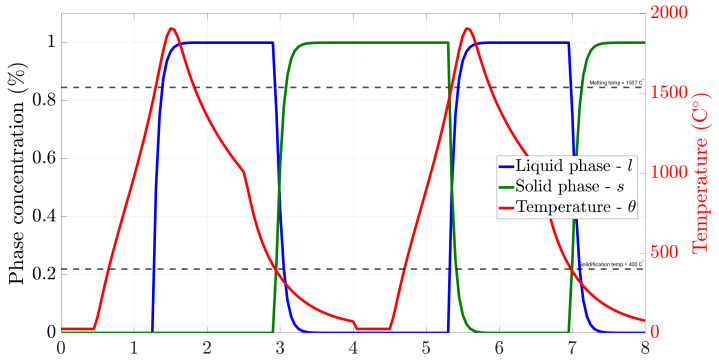

(a) $\tau_l = \tau_s$=*0.1*

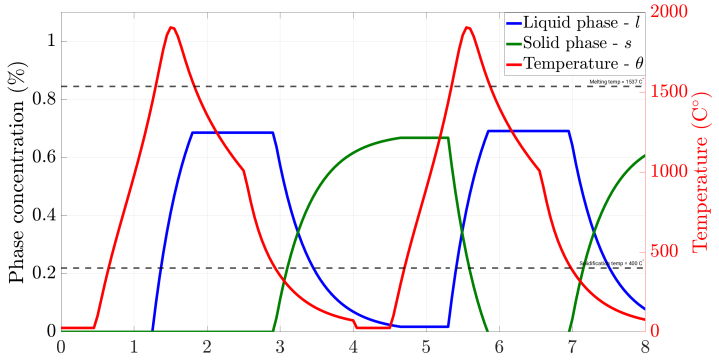

(b) $\tau_l = \tau_s$=*0.5*

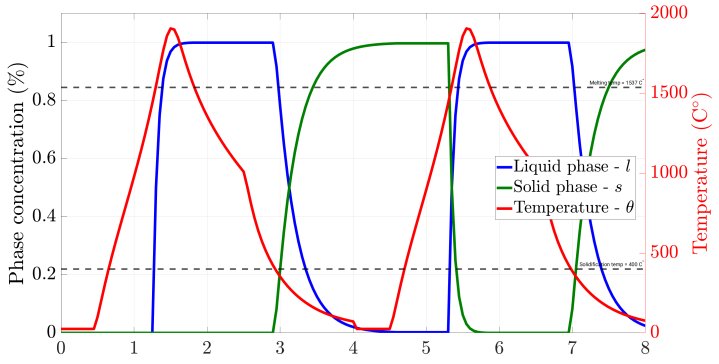

(c) τ_l=*0.1*, τ_s=*0.3*

Figure 7: *Test 3: Phase evolution vs temperature during printing process. Different values of* τ_l *and* τ_s.

Paraview results:

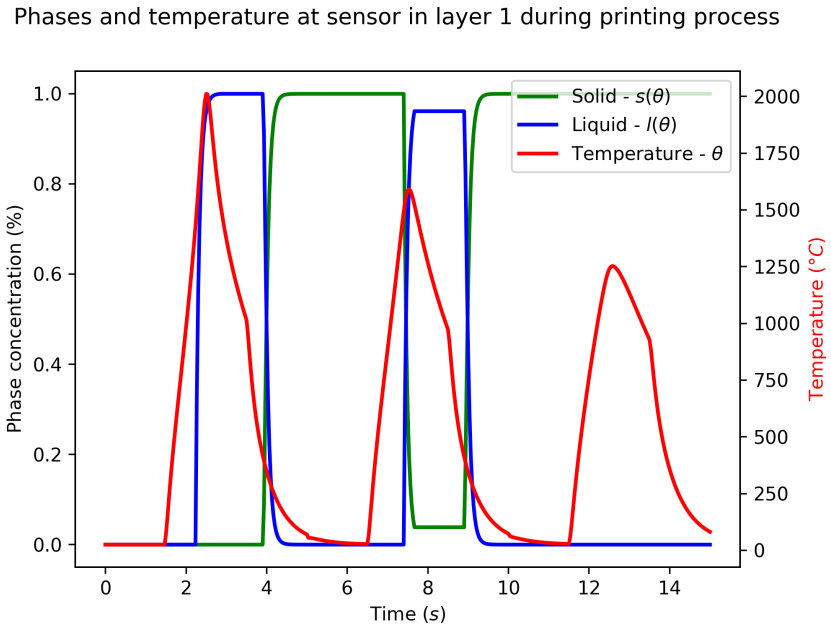

Figure 8: *Test 3: Phase evolution vs temperature during printing process of three layers.*

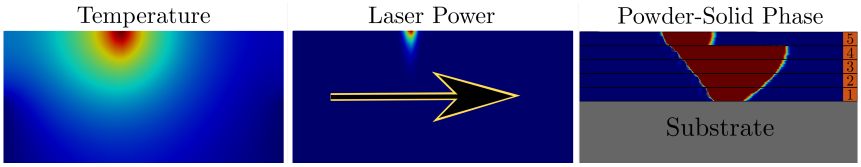

Figure 9: *Test 3: Temperature, laser power and powder and solid phase. The arrow indicates the movement of the laser. The numbers indicate the layer number.*

Videos:

- Three layers: https://tubcloud.tu-berlin.de/s/sFJJCPbQ9eD9xDt
- Five layers pyramid: https://tubcloud.tu-berlin.de/s/K25izEgAt28P4Qr

IV. Full system

XXXXXXXXXXXXXXXXXXXXXXXXXXXXXXXXXXXXXXX

V. Laser definition

The laser ϕ is the heat source in the heat equation (22). It acts on the top layer of the domain. The two aspects of the laser that must be modeled are the power distribution and movement. The power distribution around the location of the laser can be modelled in different ways: square, Gaussian, elliptical or drop (raindrop). The movement can be described as table with time and position or with an analytical expression.

Some references on Laser definition on SLM are [10, 11].

This way, as an example, we define the laser ϕ as a Gaussian distribution $\mathscr{G} = f(\mathscr{G}_c(t)) \cdot \mathscr{G}_z(z)$. The center of the Gaussian is moving according to $\mathscr{G}_c(t)$ and the decay in the z-direction is described by $\mathscr{G}_z(z)$. The Gaussian $\mathscr{G}$ is then multiplied by an "activator" function $\mathscr{P}(t)$ which indicates the power of the laser when it is on (P_0) or off (0).

$$\phi(\boldsymbol{x},t) = \exp(-\beta_1(x-\mathscr{G}_c(t))^2)\mathscr{G}_z(z)\mathscr{P}(t) \tag{36}$$

$$\mathscr{G}_c(t) = \chi_{[(i-1)\tau,\, i\tau]}(t) \cdot \left(\frac{-l}{2} + v \cdot (t-(i-1)\tau)\right) \qquad \text{for } i = 1,\ldots,n \tag{37}$$

$$\mathscr{G}_z(z) = \exp(\beta_2(z-ih)) \qquad \text{for } i = 1,\ldots,n \tag{38}$$

$$\mathscr{P}(t) = P_0 \cdot \chi_{[t_{\text{on}},\, t_{\text{off}}]}(t) \tag{39}$$

Notice that χ_Λ denotes the characteristic function of the set Λ, that is,

$$\chi_\Lambda(x) = \begin{cases} 1, & x \in \Lambda \\ 0, & x \notin \Lambda. \end{cases} \tag{40}$$

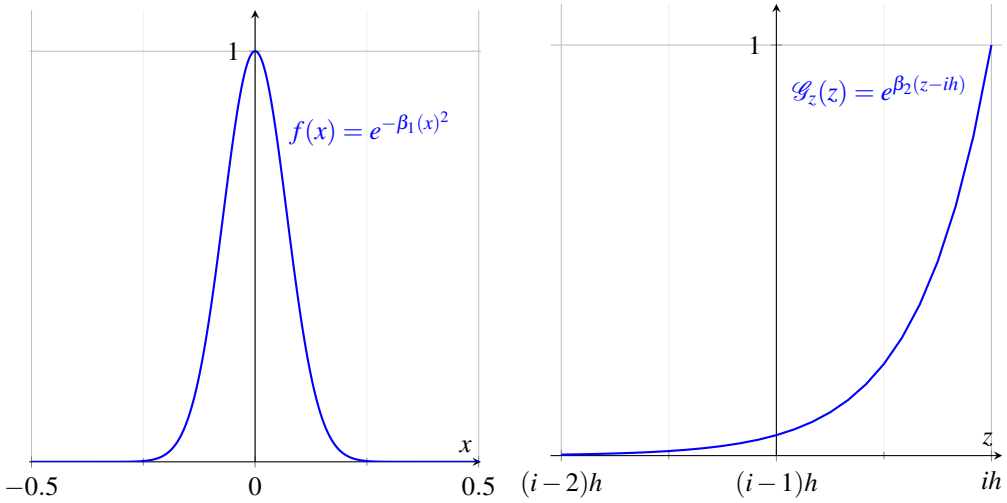

Figure 10: *Laser modelling functions f and $\mathscr{G}_z$.*

Depending on the explicit definition of t_{on} and t_{off} in (39) it is possible to control the laser path on the different layers and thus, creating different structures. A set of examples follow.

i.Square

$$t_{\text{on}} = \frac{-l_1/2 + l/2}{v} + (i-1)\tau \qquad \text{for } i = 1,\dots,n \tag{41}$$

$$t_{\text{off}} = \frac{l_1/2 + l/2}{v} + (i-1)\tau \qquad \text{for } i = 1,\dots,n \tag{42}$$

Example:

$$l_1 = 50\%l, \quad \text{being } l_1 \text{ the width of the square.} \tag{43}$$

ii.Pyramid

$$t_{\text{on}} = \frac{-l_1/2 + m(i-1) + l/2}{v} + (i-1)\tau \qquad \text{for } i = 1,\dots,n \tag{44}$$

$$t_{\text{off}} = \frac{l_1/2 - m(i-1) + l/2}{v} + (i-1)\tau \qquad \text{for } i = 1,\dots,n \tag{45}$$

Example:

$$l_1 = 40\%l, \quad \text{being } l_1 \text{ the width of the base of the pyramid,} \tag{46}$$

$$m = 20\%, \quad \text{being } l_1 \text{ the slope(?) of the pyramid.} \tag{47}$$

iii.Inverted pyramid

$$t_{\text{on}} = \frac{-l_2/2 - m(i-1) + l/2}{v} + (i-1)\tau \qquad \text{for } i = 1,\dots,n \tag{48}$$

$$t_{\text{off}} = \frac{l_2/2 - m(i-1) + l/2}{v} + (i-1)\tau \qquad \text{for } i = 1,\dots,n \tag{49}$$

Example:

$$l_2 = 8\%l, \quad \text{being } l_2 \text{ the width of the base of the inverted pyramid,} \tag{50}$$

$$m = 20\%, \quad \text{being } m \text{ the slope(?) of the pyramid.} \tag{51}$$

VI. Material properties

[12]
XXXXXXXXXXXXXXX

VII. Weak formulation

$$\rho C_p \theta_t - \nabla \cdot (\kappa \nabla \theta) = \phi \tag{52}$$

Test function φ and integrating in Ω:

$$\int_\Omega \rho C_p \theta_t \varphi \, \mathrm{d}\boldsymbol{x} - \int_\Omega \nabla \cdot (\kappa \nabla \theta)\, \varphi \, \mathrm{d}\boldsymbol{x} = \int_\Omega \phi \varphi \, \mathrm{d}\boldsymbol{x} \tag{53}$$

Using Green's formula we get:

$$-\int_\Omega \nabla\cdot(\kappa\nabla\theta)\,\varphi\,\mathrm{d}\boldsymbol{x} = -\int_\Omega (\kappa\nabla\theta)\,\nabla\varphi\,\mathrm{d}\boldsymbol{x} + \int_{\partial\Omega} -\kappa\frac{\partial\theta}{\partial n}\varphi\,\mathrm{d}s \tag{54}$$

Expanding the definition of $\partial\Omega$:

$$\begin{aligned}\int_{\partial\Omega} -\kappa\frac{\partial\theta}{\partial n}\varphi\,\mathrm{d}s = &\int_{\Gamma_i} -\kappa\frac{\partial\theta}{\partial n}\varphi\,\mathrm{d}s + \int_{\Gamma_1} -\kappa\frac{\partial\theta}{\partial n}\varphi\,\mathrm{d}s + \int_{\Sigma_1^i} -\kappa\frac{\partial\theta}{\partial n}\varphi\,\mathrm{d}s + \int_{\Sigma_2^i} -\kappa\frac{\partial\theta}{\partial n}\varphi\,\mathrm{d}s \\ &+ \int_{\Sigma_1^0} -\kappa\frac{\partial\theta}{\partial n}\varphi\,\mathrm{d}s + \int_{\Sigma_2^0} -\kappa\frac{\partial\theta}{\partial n}\varphi\,\mathrm{d}s \\ &+ \int_{\Gamma_0} -\kappa\frac{\partial\theta}{\partial n}\varphi\,\mathrm{d}s \end{aligned} \tag{55}$$

$$\begin{aligned}= &\int_{\Gamma_i} \alpha_1(\theta-\theta_a)\varphi\,\mathrm{d}x - \int_{\Gamma_1} 0\varphi\,\mathrm{d}x - \int_{\Sigma_1^i} \alpha_2(\theta-\theta_a)\varphi\,\mathrm{d}z + \int_{\Sigma_2^i} \alpha_3(\theta-\theta_a)\varphi\,\mathrm{d}z \\ &- \int_{\Sigma_1^0} 0\varphi\,\mathrm{d}z + \int_{\Sigma_1^0} 0\varphi\,\mathrm{d}z \\ &+ \int_{\Gamma_0} \alpha(\theta-\theta_s)\varphi\,\mathrm{d}x \end{aligned} \tag{56}$$

Introducing in Equation (53):

$$\begin{aligned}\int_\Omega \rho C_p\theta_t\varphi\,\mathrm{d}\boldsymbol{x} - \int_\Omega \nabla\cdot(\kappa\nabla\theta)\,\varphi\,\mathrm{d}\boldsymbol{x} = &\int_\Omega \phi\varphi\,\mathrm{d}\boldsymbol{x} - \int_{\Gamma_i} \alpha_1(\theta-\theta_a)\varphi\,\mathrm{d}x \\ &+ \int_{\Sigma_1^i} \alpha_2(\theta-\theta_a)\varphi\,\mathrm{d}z - \int_{\Sigma_2^i} \alpha_3(\theta-\theta_a)\varphi\,\mathrm{d}z \\ &- \int_{\Gamma_0} \alpha(\theta-\theta_s)\varphi\,\mathrm{d}x \end{aligned} \tag{57}$$

Time discretization for θ_t:

$$\theta_t \approx \frac{\theta^{k+1}-\theta^k}{\Delta t} \tag{58}$$

Introducing in Equation (57) and assuming $\theta \sim \theta^k$ to have a explicit scheme:

$$\begin{aligned}\int_\Omega \rho C_p\theta^{k+1}\varphi\,\mathrm{d}\boldsymbol{x} = &\int_\Omega \rho C_p\theta^k\varphi\,\mathrm{d}\boldsymbol{x} - \Delta t\int_\Omega \nabla\cdot(\kappa\nabla\theta)\,\varphi\,\mathrm{d}\boldsymbol{x} + \Delta t\int_\Omega \phi\varphi\,\mathrm{d}\boldsymbol{x} - \Delta t\int_{\Gamma_i} \alpha_1(\theta-\theta_a)\varphi\,\mathrm{d}x \\ &+ \Delta t\int_{\Sigma_1^i} \alpha_2(\theta-\theta_a)\varphi\,\mathrm{d}z - \Delta t\int_{\Sigma_2^i} \alpha_3(\theta-\theta_a)\varphi\,\mathrm{d}z \\ &- \Delta t\int_{\Gamma_0} \alpha(\theta-\theta_s)\varphi\,\mathrm{d}x \end{aligned} \tag{59}$$

Discretizing using FEM we can obtain the following matrix system for $k = 0,\ldots,N_t$:

$$\begin{aligned}\rho C_p\boldsymbol{M}\theta^{k+1} = &\rho C_p\boldsymbol{M}\theta^k - \Delta t\,\kappa\boldsymbol{K}\theta^k + \Delta t\boldsymbol{\phi} \\ &- \Delta t\boldsymbol{R}_{\Gamma_i} + \Delta t\boldsymbol{R}_{\Sigma_1^i} - \Delta t\boldsymbol{R}_{\Sigma_1^2} \\ &- \Delta t\boldsymbol{R}_{\Gamma_0} \end{aligned} \tag{60}$$

VIII. Numerical resolution

FEniCS, Domain changing with time [13, 14, 15, 16], Adaptive mesh, From 2D to 3D.

IX. Conclusions

A important reference with a similar model but for Directed Energy Deposition (DED) process is [17].

Other possible sources: [18, 19, 20, 21, 22]

References

[1] F. Dugast, P. Apostolou, A. Fernandez, W. Dong, Q. Chen, S. Strayer, R. Wicker, and A. C. To, "Part-scale thermal process modeling for laser powder bed fusion with matrix-free method and GPU computing," *Additive Manufacturing*, vol. 37, p. 101732, jan 2021.

[2] D. Hömberg, "A mathematical model for the phase transitions in eutectoid carbon steel," *IMA Journal of Applied Mathematics*, vol. 54, no. 1, pp. 31–57, 1995.

[3] ——, "A numerical simulation of the jominy end-quench test," *Acta Materialia*, vol. 44, no. 11, pp. 4375–4385, nov 1996.

[4] ——, "Irreversible phase transitions in steel," *Mathematical Methods in the Applied Sciences*, vol. 20, no. 1, pp. 59–77, jan 1997.

[5] J. Fuhrmann and D. Hömberg, "Numerical simulation of the surface hardening of steel," *International Journal of Numerical Methods for Heat & Fluid Flow*, vol. 9, no. 6, pp. 705–724, sep 1999.

[6] D. Hömberg, "A mathematical model for induction hardening including mechanical effects," *Nonlinear Analysis: Real World Applications*, vol. 5, no. 1, pp. 55–90, feb 2004.

[7] D. Hömberg and W. Weiss, "PID control of laser surface hardening of steel," *IEEE Transactions on Control Systems Technology*, vol. 14, no. 5, pp. 896–904, sep 2006.

[8] D. Hömberg, Q. Liu, J. Montalvo-Urquizo, D. Nadolski, T. Petzold, A. Schmidt, and A. Schulz, "Simulation of multi-frequency-induction-hardening including phase transitions and mechanical effects," *Finite Elements in Analysis and Design*, vol. 121, pp. 86–100, nov 2016.

[9] D. Koistinen and R. Marburger, "A general equation prescribing the extent of the austenite-martensite transformation in pure iron-carbon alloys and plain carbon steels," *Acta Metallurgica*, vol. 7, no. 1, pp. 59–60, jan 1959.

[10] J. Ning, E. Mirkoohi, Y. Dong, D. E. Sievers, H. Garmestani, and S. Y. Liang, "Analytical modeling of 3d temperature distribution in selective laser melting of ti-6al-4v considering part boundary conditions," *Journal of Manufacturing Processes*, vol. 44, pp. 319–326, aug 2019.

[11] E. Mirkoohi, D. E. Seivers, H. Garmestani, and S. Y. Liang, "Heat source modeling in selective laser melting," *Materials*, vol. 12, no. 13, p. 2052, jun 2019.

[12] L.-E. Loh, C.-K. Chua, W.-Y. Yeong, J. Song, M. Mapar, S.-L. Sing, Z.-H. Liu, and D.-Q. Zhang, "Numerical investigation and an effective modelling on the selective laser melting (SLM) process with aluminium alloy 6061," *International Journal of Heat and Mass Transfer*, vol. 80, pp. 288–300, jan 2015.

[13] M. Gouge, E. Denlinger, J. Irwin, C. Li, and P. Michaleris, "Experimental validation of thermo-mechanical part-scale modeling for laser powder bed fusion processes," *Additive Manufacturing*, vol. 29, p. 100771, oct 2019.

[14] M. Chiumenti, E. Neiva, E. Salsi, M. Cervera, S. Badia, J. Moya, Z. Chen, C. Lee, and C. Davies, "Numerical modelling and experimental validation in selective laser melting," *Additive Manufacturing*, vol. 18, pp. 171–185, dec 2017.

[15] M. Bayat, C. G. Klingaa, S. Mohanty, D. D. Baere, J. Thorborg, N. S. Tiedje, and J. H. Hattel, "Part-scale thermo-mechanical modelling of distortions in laser powder bed fusion – analysis of the sequential flash heating method with experimental validation," *Additive Manufacturing*, vol. 36, p. 101508, dec 2020.

[16] C. Baykasoğlu, O. Akyildiz, M. Tunay, and A. C. To, "A process-microstructure finite element simulation framework for predicting phase transformations and microhardness for directed energy deposition of ti6al4v," *Additive Manufacturing*, vol. 35, p. 101252, oct 2020.

[17] D. Weisz-Patrault, "Fast simulation of temperature and phase transitions in directed energy deposition additive manufacturing," *Additive Manufacturing*, vol. 31, p. 100990, jan 2020.

[18] N. E. Hodge, R. M. Ferencz, and J. M. Solberg, "Implementation of a thermomechanical model for the simulation of selective laser melting," *Computational Mechanics*, vol. 54, no. 1, pp. 33–51, apr 2014.

[19] Q. Chen, G. Guillemot, C.-A. Gandin, and M. Bellet, "Three-dimensional finite element thermomechanical modeling of additive manufacturing by selective laser melting for ceramic materials," *Additive Manufacturing*, vol. 16, pp. 124–137, aug 2017.

[20] Y. Yang, M. Knol, F. van Keulen, and C. Ayas, "A semi-analytical thermal modelling approach for selective laser melting," *Additive Manufacturing*, vol. 21, pp. 284–297, may 2018.

[21] R. Yavari, R. Williams, A. Riensche, P. A. Hooper, K. D. Cole, L. Jacquemetton, H. S. Halliday, and P. K. Rao, "Thermal modeling in metal additive manufacturing using graph theory – application to laser powder bed fusion of a large volume impeller," *Additive Manufacturing*, vol. 41, p. 101956, may 2021.

[22] R. Yavari, Z. Smoqi, A. Riensche, B. Bevans, H. Kobir, H. Mendoza, H. Song, K. Cole, and P. Rao, "Part-scale thermal simulation of laser powder bed fusion using graph theory: Effect of thermal history on porosity, microstructure evolution, and recoater crash," *Materials & Design*, vol. 204, p. 109685, jun 2021.